Chalcogenide Letters Vol. 21, No. 11, November 2024, p. 917 - 926

# High optimization of crystallization experimental conditions of ZnO nano thin films prepared by spray pyrolysis technique for optoelectronic applications

L. Bouras [a], A. Beggas [a,*], D. Sahnoune [b], M. Ghougali [a], R. Ferhat [a]
[a] *LEVRES Laboratory, University of El Oued, 39000 El Oued, Algeria*
[b] *Plateau technique en analyses physico-chimiques PTAPC.CRAPC-Biskra 07000 Algeria*

The present study intends to provide the impact of nitric acid on the structural and optical characteristics of thin films of ZnO. The latter was grown on substrates of glass via spray pyrolysis with 400°C, using Zinc acetate aqueous solution acidified by different amounts of nitric acid to obtain a pH ranging from 6.8 to 2.9. The film properties were analyzed as a function of pH. In the light of the XRD analysis, all the films have a preferential direction along the (002) plane. Depending on pH conditions, the crystal size increased from 32.38 to 37.4 nm, with a decrease in pH from 6.8 to 2.9, according to the X-ray diffraction analysis. It can be observed from the transmission spectra of the 300-900 nm wavelengths range that the optical transmission of the films is on average above 90%, and band gap values were found in the range 3.28 - 3.19 eV. The ZnO film's FTIR spectrum in the wavenumber range (400-4000 $cm^{-1}$) displayed a wide band between 400 and 552 $cm^{-1}$, which was assigned to the Zn-O stretching mode.

(Received July 21, 2024; Accepted November 11, 2024)

*Keywords:* ZnO films, pH, Spray pyrolysis deposition, Optical and structural properties

## 1. Introduction

The chemical spray pyrolysis method is one of the major techniques used to deposit various categories of materials such as metals and alloy oxides. Zinc oxide is a multipurpose compound semiconductor material known for its outstanding characteristics and wide range of applications in electronics, optoelectronics, photonics, catalysis, sensors, and biological fields [1-3]. ZnO thin films have gained considerable attention for their capability to be tailored for high infrared reflectance, superior electrical conductivity, and excellent visible transmittance using various coating methods [4]. The noticeable properties of ZnO are due to its high transmission in the visible range and wide direct bandgap of 3.37 eV, ZnO films are capable of replacing ITO and $SnO_2$ due to their optical and electrical properties and proven stability as previously mentioned [5]. Metal-organic chemical vapor deposition [6], radio frequency sputtering [7], spin-coating [8], pulsed laser deposition [9], physical vapor deposition [10], hydrothermal [11], and spray pyrolysis [12] are amongst the techniques used for depositing ZnO films. However, some of these methods require very expensive and complex experimental equipment. So, a lower-charge and facilitated production way to deposit ZnO films using spray pyrolysis has been developed. The use of the latter method brings numerous benefits regarding repeatability, trustworthiness, and ease of controlling compounds. The properties of ZnO thin films, including their structural, optical, and chemical aspects, are greatly impacted by variables like temperature, solvents, time, and precursors, etc. Thus, it's important to study the impact of the deposition solution pH on the structural, morphological, and optical characteristics of ZnO samples. Former investigators have discussed the impact of various solvents, isopropyl alcohol (IPA), methanol (MeOH), 2-methoxy ethanol (2-ME), and ethanol (EtOH) on the ZnO samples characteristics fabricated using sol-gel spin-coating technique. It was noticed that ZnO film prepared with 2-ME has elevated transmittance (more than 90%), a wide bandgap of 3.28 eV, and 3.131nm as surface roughness [13]. The growth of Wurtzite ZnO nanostructures is achieved under different pH values ranging from 1-12 (acidic to basic) via a hydrothermal method, accompanied by post-

* Corresponding author: azzeddine-beggas@univ-eloued.dz
https://doi.org/10.15251/CL.2024.2111.917

annealing to alleviate defects arising from processing at low temperatures, the ZnO nanostructures morphology varied from nanopompons, nanorods, and nano-flowers while raising at acidic, neutral, and basic solutions, in the order indicated [11]. ZnO samples prepared by spray pyrolysis under pH conditions from pH=2 to pH=5 at 400°C, films prepared at higher pH values were found to be less compact compared with those prepared at lower values, all the films were zincite-like with preferred structural orientation (0 0 2) [12]. A few works have been published on the influence of the acidity gradient of undoped ZnO (drop by drop) on the optical properties. In this work, the spray pyrolysis approach was used for preparing ZnO samples on a glass substrate using a deposition solution with different pH values (pH=6.8 to pH=2.9). This work intents to research the impact of the acidity on the chemical composition, structural, and optical characteristics of these samples.

## 2. Experimental procedure

Zinc oxide samples were fabricated on a standard glass substrate in a homemade system using spray pyrolysis. The temperature was fixed at 400°C, the flow orientation was perpendicular to the horizontal face of the substrate, the space from the nozzle to the substrate was fixed at 30 Cm, and the air pressure of 0.5 bar, the solution flow rate was adjusted to be 10 ml/min. Zinc acetate Zn $(CH_3COO)_2 \cdot 2H_2O$ was utilized as a source substance to prepare Zn-solutions. The spray solution was obtained by solving (0.1M) of zinc acetate dihydrate in 20 ml of bi-distilled water, the mixture was agitated by magnetic agitate for 1h at 30°C. Consequently, a transparent and homogeneous solution was obtained. Eq (1) gives the chemical reaction that occurs in spray pyrolyzed liquid zinc acetate precursor.

$$[Zn(CH_3COO)_2.2H_2O] + 2H_2O_{(aq)} \xrightarrow{\Delta} ZnO_{(l)} + 2CO_{2_{(g)}} + 2CH_{4_{(g)}} + H_2O_{(g)}$$

The pH of the obtained solution was 6.8, and then nitric acid ($HNO_3$) with different volumes was appended to the former solution to get spray solutions together with various pH values (4.6, 4.4, 4.1, 3.8, and 2.9). The pH values were measured and controlled using a pH meter. To prevent any kind of contamination, before each reading the pH meter should be cleaned.

### 2.1. Sample preparation

Ordinary slide glasses were employed as substrates. In this technique, substrate purifying plays a substantial part in the deposition of thin films and the well-adherence of the film on the substrate surface. For these reasons, the substrates were initially cleaned with detergent, then rinsed in an ethanol solution, after that scoured with acetone, and finally rinsed with deionized water for more than 15 min before the procedure of deposition. The slides were dried with a dryer to eliminate the moisture from the substrate surface, avoiding touching the substrate surface to avert any contamination.

### 2.2. Characterization techniques

The structural characterization was executed by X-ray diffraction (XRD, Bruker D 8 advance X-ray diffractometer) with CuK_(α) (λ=1.5418Å). The angle of scanning (2θ) value was between (20 and 80°). The optical transmittance was studied using a UV-visible (Spectrophotometer, Shimadzu, Model 1800) working within 300-900 nm. The surface roughness and morphology were defined with the use of scanning electron microscopy. Atomic force microscopy (AFM, Park Scientific Instrument Auto Probe model CP) analysis was carried out utilizing the force constant mode to investigate the deposited film's topographical information. Fourier transform infrared (FTIR) spectrum were registered utilizing (Shimadzu spectrometer IR affinity type-1) functioning in the range (400-4000) $cm^{-1}$.

## 3. Results and discussion

### 3.1. X-ray diffraction analysis

XRD spectra of ZnO films are presented in Figure 1. The X-ray diffraction data was recorded over 2θ domain from 20 to 80°. All the prepared ZnO films are extremely textured, together with the c-axis perpendicularly on the film surface. The outcomes prove that all the films have a wurtzite hexagonal structure and a preferential growing along (0 0 2) direction at the position of 2θ=34,4° with a little grown peak at 2θ=36,3° which attributed to the crystal plane (101) according to the standard JCPDS card of the wurtzite hexagonal structure. The tight peaks confirm that the films have excellent crystallinity, have a strong predilection to be oriented along the (002) plane, and their intensity is fundamentally related to the pH value. It is worth noting that the crystallinity increased (peak intensity) as the pH decreased from 4.6 to 3.8 to reach its maximum at pH=3.8 and then, decreased at pH=2.9. In other words, the intensity and sharpening of this peak increased, which is induced by an amelioration in the crystallinity of the film if 3.8≤pH≤4.6. A previous study reported that the deposition rate is important in the case that 3.5≤pH≤4.3, which gives rise to an enlargement in the thickness of the film and the crystallite size [14]. Furthermore, it is noticed the appearance of small peaks at 2θ=31.68°, 47.47°, 62.70°, and 72.48° correspond to the following planes (100), (102), (103), (004) as reported in the literature [15] for pH values ranging from 4,4 to 2,9. All the diffraction peak positions follow the standard card (JCPDS card: No 36-1451). The XRD spectra of ZnO have no diffraction peaks other than ZnO, which indicates the absence of any impurity phase, revealing the best quality of the films.

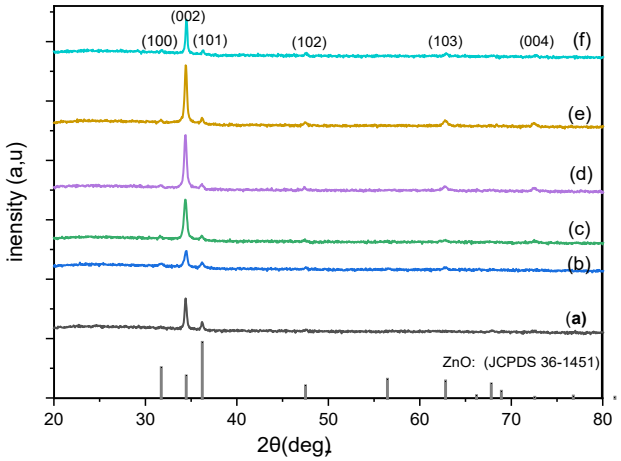


*Fig. 1. XRD Patterns of ZnO films at diverse pH values at substrate temperature of 400°C.*

The crystallite size $\boldsymbol{D}$ of all the films along c-axis was figured using the Debye–Scherrer formula:

$$D = \frac{k\lambda}{\beta cos\theta} \tag{1}$$

The Scherrer constant $\boldsymbol{k}$=0.9, while λ represents the incident X-ray radiation wavelength ($\boldsymbol{\lambda}$ = 1.5406 nm). $\boldsymbol{\beta}$ represents the (FWHM), and $\boldsymbol{\theta}$ is the diffraction angle of Bragg. The estimated crystallite sizes, utilizing Equation 1, are summarized in Table 1. The crystal sizes range from 32.38 to 37.8 nm. The results show that the ZnO film obtained at pH=6.8 has the littlest crystallite size (32.38 nm), while film prepared at pH=2.92 presented the largest crystalline size (37.8 nm), that phenomenon was reported [16], the results follow the SEM and AFM findings, as we will see later. Since the crystallite size is conversely proportional to the (FWHM), the crystallite size is raised as

the (FWHM) is reduced. It is noticed that the intensities of the (002) peaks rise as their FWHM values constrict, which indicates an amelioration in the film crystallinity. The augmentation of the size of crystallite has been mentioned by the crystallinity improvement and c-axis direction of ZnO films [17].

By applying the Bragg condition (Eq.2), it is possible to make an estimation of the inter-planar spacing $\boldsymbol{d_{hkl}}$based on the X-ray diffraction profiles.

$$2d_{hkl}sin\theta = n\lambda \tag{2}$$

where $\boldsymbol{n}$ is the diffraction order, whereas ($\boldsymbol{hkl}$ ) are the Miller planes indices, and $\boldsymbol{\theta}$ is the Bragg angle. The predestined values of $\boldsymbol{d_{hkl}}$ spacing are summarized in Table 1. These obtained values matched very much with those of the (JCPDS card: No 36-1451) data for hexagonal ZnO.

The lattice constant '$\boldsymbol{a}$' and '$\boldsymbol{c}$', for the hexagonal phase are estimated by the following equation [18]:

$$\frac{1}{d_{hkl}^2} = \frac{l^2}{c^2} + \frac{4}{3}\left(\frac{h^2 + hk + k^2}{a^2}\right) \tag{3}$$

Lattice parameters of the unit cell were calculated at the (002) plane and listed in Table 1. As can be observed, the $\boldsymbol{c}$ '' and $\boldsymbol{a}$ of the unit cell are almost constant and give a $\boldsymbol{c/a}$ ratio nearly equal to 1.60. It is close to an ideal hexagonal structure ratio, which is recorded as 1.63. It reflects the best compactness of the films [15].

To give more information about detailed structure, dislocation densities for all the samples were estimated, using the relation below and are given in Table 1.

$$\delta = \frac{1}{D^2} \tag{4}$$

where $\boldsymbol{\delta}$ is the dislocation density. It is clear that larger $\boldsymbol{D}$ values correspond to smaller $\boldsymbol{\delta}$ values. These values exhibit that the solution pH affects the dislocation density of the ZnO samples. Increasing the acidity of the solution (decrease of pH value) resulted in a reduce in dislocation density, which shows that decreasing pH reduced the crystal lattice defects.

*Table 1. Micro-structural parameters of Zinc Oxide films obtained by different pH values.*

| pH | 2θ | (hkl) | d (nm) | FWHM | a (nm) | c (nm) | c/a | D (nm) | $\delta*10^{-3}$ |
|---|---|---|---|---|---|---|---|---|---|
| pH=6.8 | 34,4 | (002) | 0,26 | 0,256 | 0,3231 | 0,5173 | 1,603 | 32.38 | 0.950 |
| pH=4,6 | 34,43 | (002) | 0,2601 | 0,255 | 0,3237 | 0,5176 | 1,599 | 32.61 | 0.947 |
| pH=4,4 | 34,4 | (002) | 0,2605 | 0,244 | 0,3238 | 0,5175 | 1,598 | 33.67 | 0.880 |
| pH=4,1 | 34,41 | (002) | 0,2605 | 0,241 | 0,3239 | 0,5176 | 1,598 | 34,5 | 0,831 |
| pH=3,8 | 34,42 | (002) | 0,2604 | 0,222 | 0,3239 | 0,5176 | 1,598 | 37,4 | 0,712 |
| pH=2,9 | 34,48 | (002) | 0,259 | 0,219 | 0,3239 | 0,5178 | 1,600 | 37.8 | 0,690 |

The difference between the estimated lattice parameter '$\boldsymbol{c}$' and the standard one of the bulk sample ($\boldsymbol{c_0} = 0.5206\ nm$) shows that the prepared films were under strain. The strain along the c-axis for all the films was estimated from the relation underneath [19]:

$$\epsilon = \frac{\beta cos\theta}{4} \tag{4}$$

where $\boldsymbol{\beta}$ represents the (FWHM) of a defined diffraction peak and $\boldsymbol{\theta}$ is the angle of Bragg. It is marked that the micro-strain ϵ shows a gradually decreasing tendency with a decrease in pH. The

reduction in the strain as film thickness grows indicates a decrease in the coherent force amidst film and substrate, reflecting an enlargement in crystallite size and a lowering in lattice imperfections.

**3.2. SEM results**

The prepared thin films surface morphology was examined by SEM micrographs. Figure 2. presents the surface topography SEM micrographs of the films prepared at diverse pH values. The latter confirms that the thin films microstructure changes with the starting solution pH values. The obtained images from scanning electron microscopy show that the grain size grows and its homogeneity rises when the acidity of the deposition solution is raised (pH decreased). The same behavior was reported by R. Wahab et al. [20]. Rounded grains are observed in all the micrographs. It's worth noting that above the entire glass substrate, all the films have a uniform surface morphology.

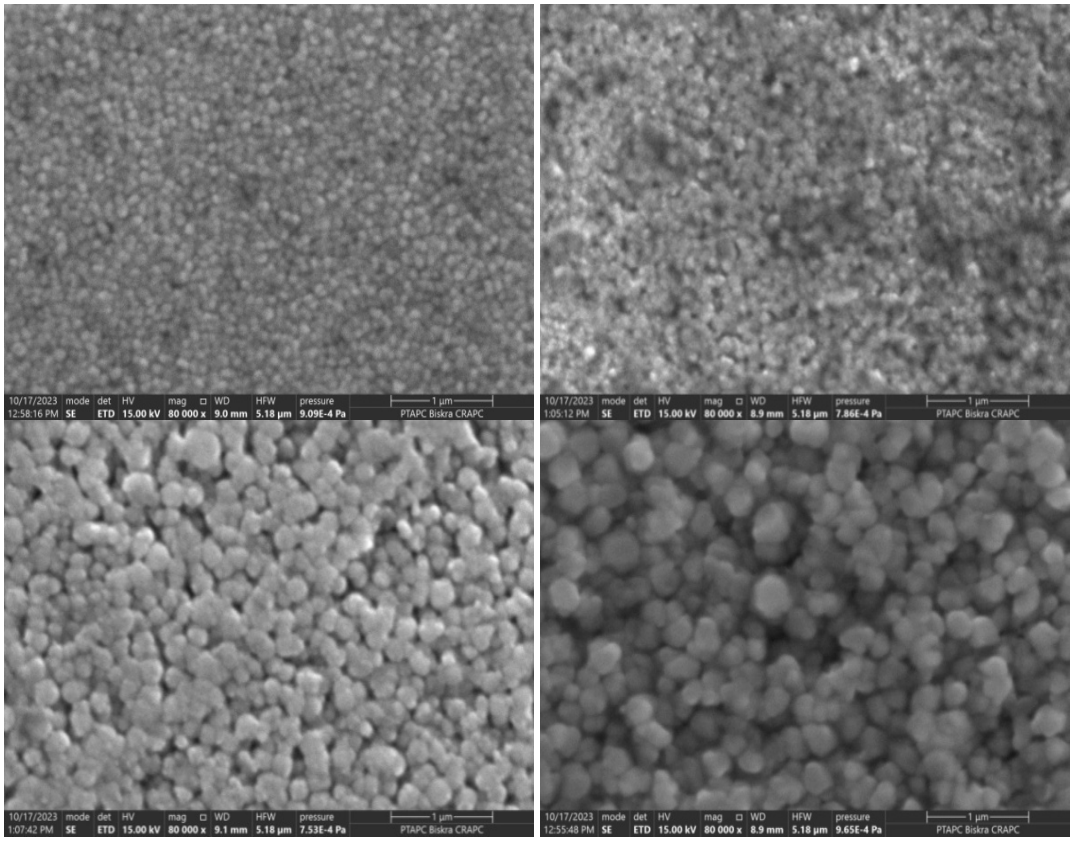


*Fig. 3. Scanning electron micrographs of ZnO films for: (a). pH=6.8, (b). pH=4.6, (c). pH=4.4, (d). pH=3.8.*

**3.3. AFM results**

Atomic force microscopy offers the most diverse and powerful method for analyzing samples at the nanoscale level [21]. An AFM generates images by scanning a cantilever over the surface of a sample. Two-dimensional AFM pictures of ZnO films, scanning a region of the film surface prepared with different pH of starting solutions, are shown in Fig. 4. The surface presents a recognizable grain distribution with compact granular topography. It also confirms the impact of the starting solution pH on the crystallite size. The latter decreases when the pH increases. The grain presents the sphere shape with homogenous and uniform distribution on the surface. In higher pH, a lot of grains' random distribution on the surface is observed, which leads to a higher roughness.

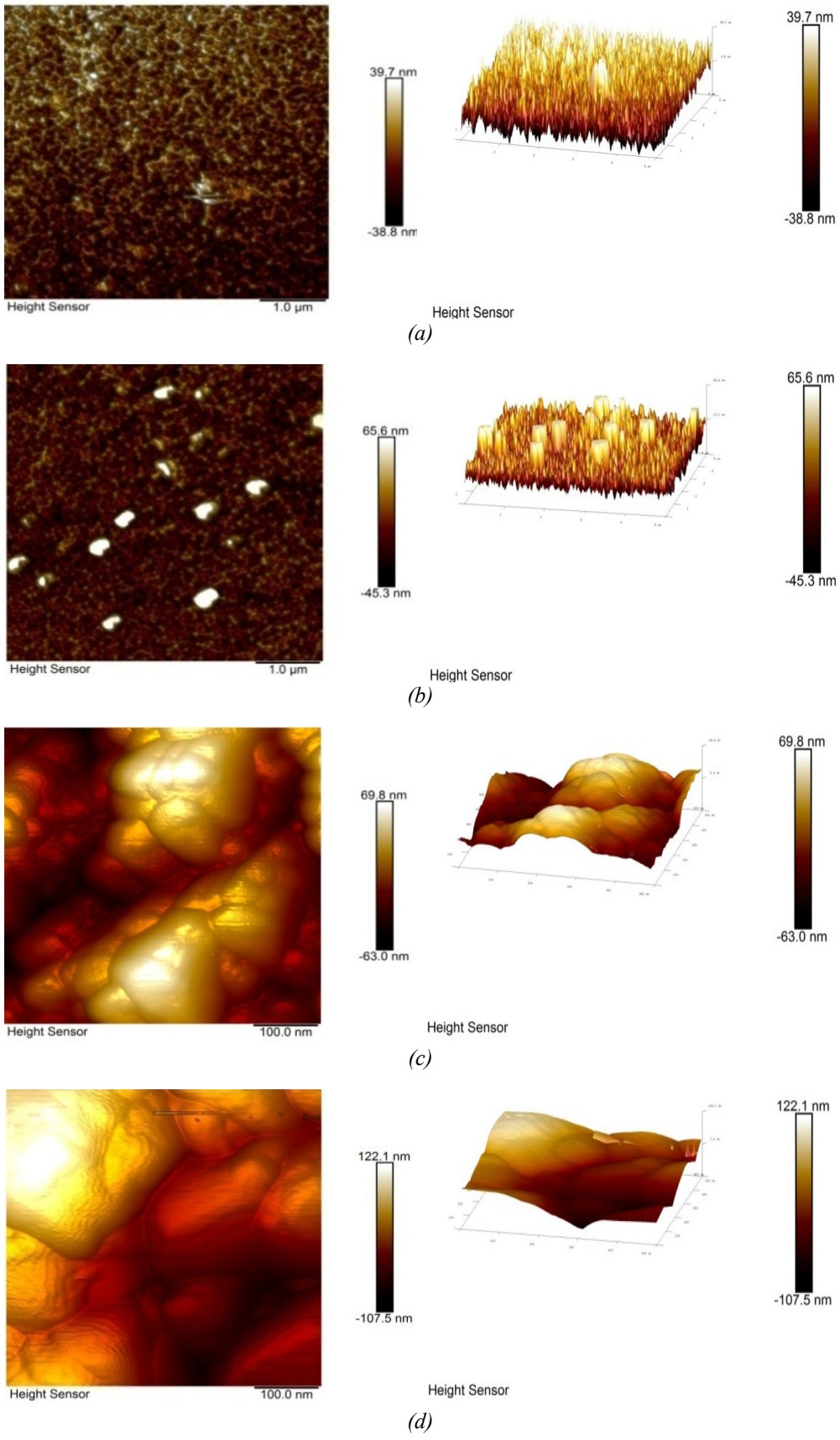


*Fig. 4. 2D AFM images of ZnO samples for: (a). pH=6.8, (b). pH=4.6, (c). pH=4.1, (d). pH=3.8.*

### 3.4. Optical properties

UV-Vis spectroscopy has been utilized to investigate the impact of different pH values on optical characteristics, such as energy band gap, transmittance, and band tail width. The optical transmission curves of ZnO samples recorded as a function of wavelength on the spectrum from 300 to 900 nm are presented in Figure. 5. It is clear that the Transmission characteristics were dependent on the acidity of the spray solution (pH value) for the set samples studied. All the films show more than 80% transmission for wavelengths longer than 400 nm. It is observed that the transmission for the case of pH=6.8 and pH=4.6-based films is better than other films. As one can see in Figure. 5, that transmittance rises rapidly above 80% for wavelengths above 400 nm. While below 400 nm, there is an acute drop-down in the transmittance proportion of the films, indicating a strong absorption in this range. That may be due to rapid change in the optical absorption coefficient, indicating that some states have been formed in the zone between the two bands valence and conduction.[22]. The transmittance reduction at smaller pH values may be referred to as the augmented scattering of photons by expanding the surface morphology roughness. In addition, the transmission values decrease with pH values, which may be due to the increased surface roughness. A similar observation was reported [23].

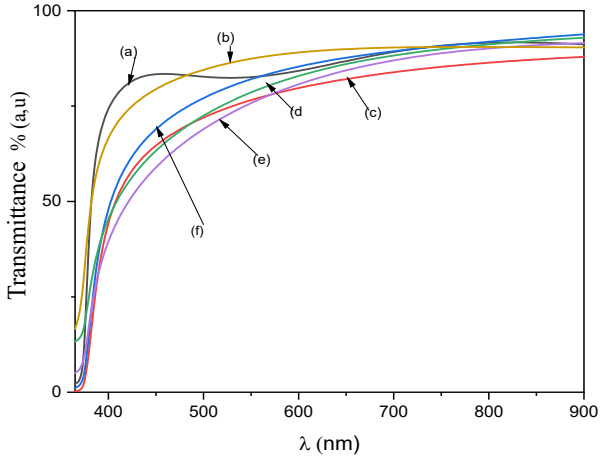


*Fig. 5. Optical transmittance of ZnO films for:*
*(a) pH=6.8, (b) pH=4.6, (c) pH=4.4, (d) pH=4.1, (e) pH=3.8, (f) pH=2.9.*

The band gap of semiconductor materials is considered one of the more valuable parameters for optical and electrical applications. Analyzing the optical transmittance data versus wavelength can provide significant insights including band gap. Corresponding to Tauc's equation for direct band gap semi-conductors [20], the latter can be estimated from the plot of $(\alpha h\nu)^2$versus $(h\nu)$as shown in Figure 6.

With a decrease in pH from pH=6.8 to pH=3.8, the band gap decreased from 3,28 to 3,19 eV. The lowering in the bandgap energy with a rise in acidity may be due to an addition in carrier concentration or a reduction in strain values. The relation between the compressive stress of the ZnO films and the direct bandgap has been reported in the literature. In addition, a prior study found that the bandgap enlarges when particle size reduces [24]. Urbach energy can be calculated from the plot of log(α) versus (hυ). The latter is a consequence of the disorder in the sample. The Urbach energy of the ZnO film increases somewhat from 67 to 192 meV when the pH values reduced from 6.8 to 3.8, then decreases to 151meV at pH=2.9, as shown in Table 2. As can be seen, the variation of the disorder is opposed to the band gap ones. This attitude shows clearly that the band gap in the deposited films is ruled by the disorder variation. Moreover, Urbach energy findings are referred to as result of thermal instabilities and structural flaws. The variation in the band tail characteristic underscores the importance of solution concentration as a defect source inside the ZnO lattice [25].

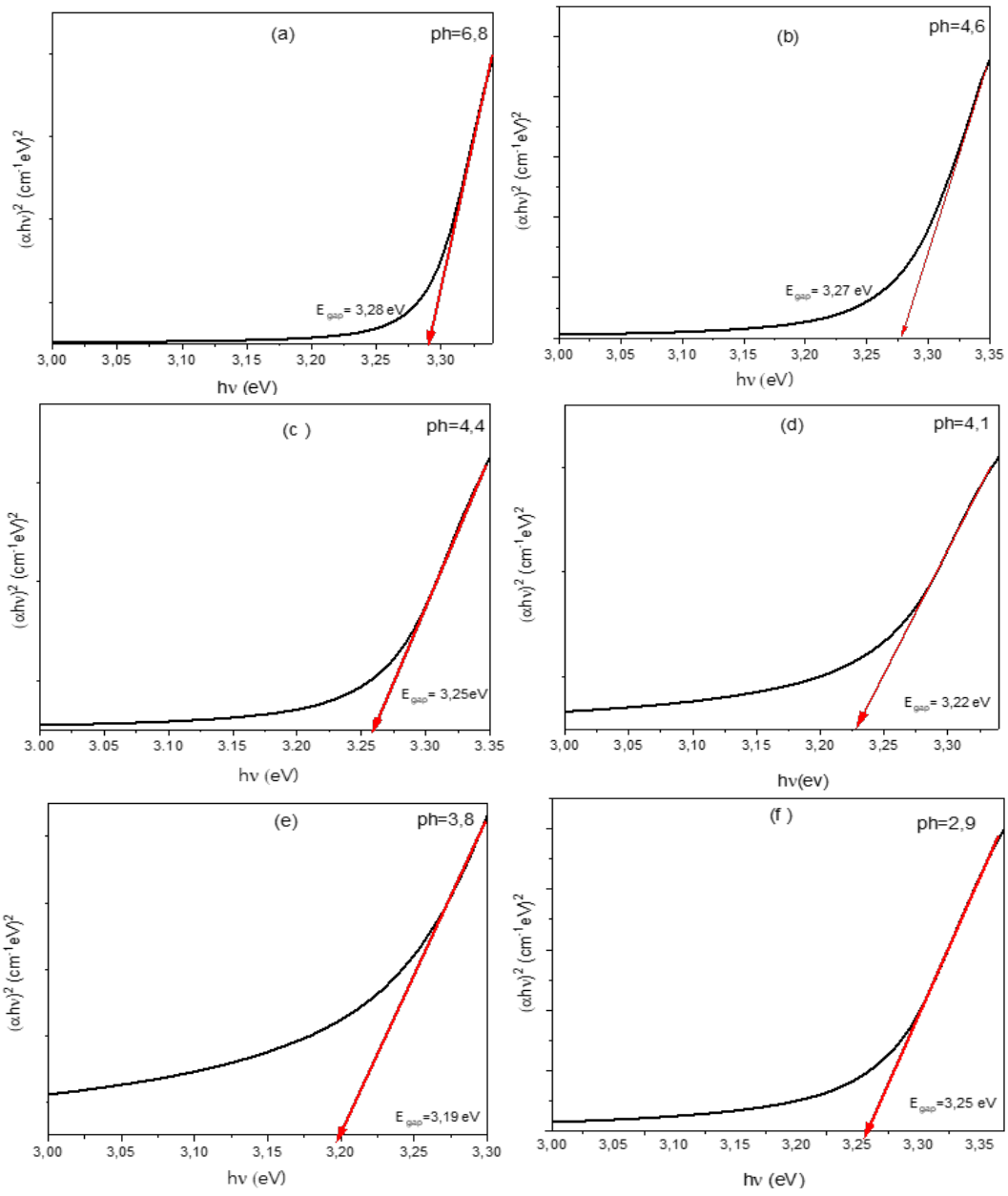


*Fig. 6. Tauc's plot of ZnO films.*

*Table 2. Shows the values of band gap and Urbach energies of ZnO films.*

| pH | Eg Band gap (eV) | EU (meV) |
|---|---|---|
| pH=6.8 | $E_g$=3.28 eV | $E_U$=67 meV |
| pH=4.6 | $E_g$=3.27 eV | $E_U$=103 meV |
| pH=4.4 | $E_g$=3.25 eV | $E_U$=107 meV |
| pH=4.1 | $E_g$=3.22 eV | $E_U$=149 meV |
| pH=3.8 | $E_g$=3.19 eV | $E_U$=192meV |
| pH=2.9 | $E_g$=3.25 eV | $E_U$=151 meV |

### 3.5. FTIR measurement

FTIR spectral analysis was utilized to determine the functional groups of the prepared nanostructured ZnO films. Fig. 8 shows the FTIR spectra of all the ZnO samples over 400 $Cm^{-1}$ to 4000 $Cm^{-1}$. The absorption peaks at 443, 446, and 449 $Cm^{-1}$ in different films grown at various pH

values are assigned to the Zn–O stretching mode of vibration. The change in characteristic peak locus may be due to variance in crystallinity, shape, or particle size. It's noticed that as the solution pH decreases, there is a tiny shift of the peak at higher frequencies. This change is analogous to SEM and AFM observations. While the vibrational peaks appeared in a range from 1700 to 600 $Cm^{-1}$ are imputed to C=O, C-O, and C-H vibrations. Peaks at 742 $Cm^{-1}$ is imputed to C–C stretching. The absorption peak at 879 $Cm^{-1}$ indicates the presence of C = C functional group. Moreover, absorption peaks at 2847 $Cm^{-1}$ and 2922 $Cm^{-1}$ bands imply the presence of symmetrical and asymmetrical C–H bond. Additionally, the wide absorption peak band at around 3400 $Cm^{-1}$ is assigned to the O–H (hydroxyl) stretching vibrations.

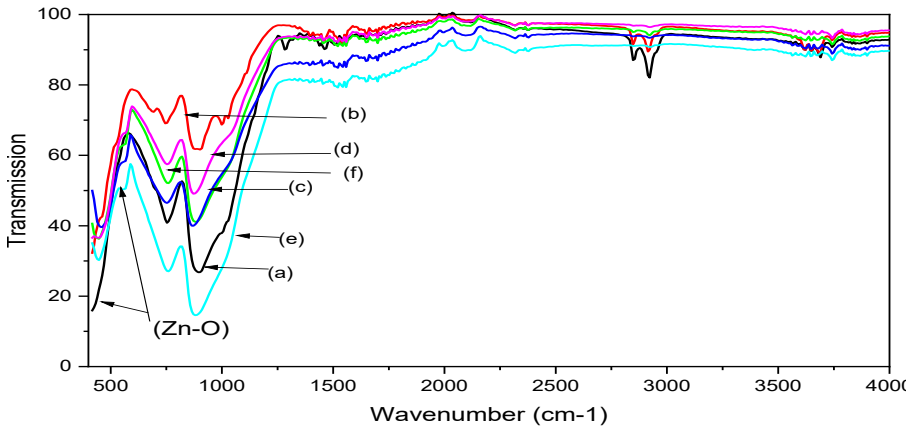


*Fig. 8. Typical FTIR spectra of ZnO thin films at different pH values.*

## 4. Conclusions

Samples of ZnO were successfully fabricated on a substrate of glass using spray pyrolysis with different values of the initial solution pH and 400°C. Zinc acetate $Zn(CH_3COO)_2{\cdot}2H_2O$ was used as source of zinc, while nitric acid solution served as a modification agent to modify the pH of the solution. The XDR data indicates that ZnO thin films have a hexagonally wurtzite structure, that has a predilected orientation along the (002) axis. The distribution of ZnO crystallites is uniform and increases with a decrease in pH. Optical properties were extensively investigated in the wavelength domain (300 to1100) nm. The transmittance decreases slightly when the value of pH decreases, and it's high than 80% for all the samples. The bandgap energy was estimated and was found in the range of 3.29 - 3.19 eV. The results show that pH has a notable impact on both structural and optical properties. XRD analysis showed an excellent crystallinity of the ZnO samples deposited for $3.8 \leq pH \leq 4.6$.

## References

[1] U. Ozgur, Y. I. Alivov, C. Liu, A. Teke, M. A. Reshchikov, S. Dogan, V. Avrutin, S. J. Cho, H. Morkoc, J. Appl. Phys, **98**(4), 041301, (2005); https://doi.org/10.1063/1.1992666
[2] N. Karak, P. K. Samanta, T. K. Kundu, Optik, **124** (23), 6227–6230, (2013); https://doi.org/10.1016/j.ijleo.2013.05.019
[3] J. G. Cuadra, A. C. Estrada, C. Oliveira, L. A. Abderrahim, S. Porcar, D. Fraga, T. Trindade, M. P. Seabra, J. Labrincha, J. B. Carda, Ceramics International, **49** (20), 32779-32788, (2023) ; https://doi.org/10.1016/j.ceramint.2023.07.246
[4] N. A. Sultanov, Z. X. Mirzajonov, F. T. Yusupov, & T. I. Rakhmonov, East European Journal of Physics, **2**, 309-314, (2024) ; https://doi.org/10.26565/2312-4334-2024-2-35

[5] C. Gumu, O. M. Ozkendir, H. Kavak, Y. Ufuktpe, Journal of Optoelectronics and Advanced Materials, **8** (1), 299 - 303 (2006); https://www.researchgate.net/publication/280137343
[6] P. H. Lei, C-H. Cheng, Materials Science in Semiconductor Processing, **57**, 220-226, (2017); https://doi.org/10.1016/j.mssp.2016.09.039
[7] E. Sener, O. Bayram, U. Hasar, O. Simsek, Physica B: Condensed Matter, **605**, 412-421, (2021); https://doi.org/10.1016/j.physb.2020.412421
[8] A. Zaidi, K. Tiwari, R. R. Awasthi, K. C. Dubey, Chalcogenide Letters, **20** (1), 33-41, (2023); https://doi.org/10.15251/CL.2023.201.33
[9] H. S. Kim, J. M. Erie, S. J. Pearton, D. P. Norton, F. Ren, Appl. Phys. A ,**91**, 251–254, (2008); https://doi.org/10.1007/s00339-008-4426-1
[10] A. Krzesinski, Thin Solid Films, **138**(1), 111-120, (1986); https://doi.org/10.1016/0040-6090(86)90221-X
[11] A. Rayerfrancis, P. B. Bhargav, N. Ahmed, B. Chandra, S. Dhara, Physica. B, **457**, 96–102, (2015); http://dx.doi.org/10.1016/j.physb.2014.09.044
[12] M. Quintana, E. Ricra, J. Rodrıguez, W. Estrada, Catalysis Today, **76**, 141–148, (2002) ; https://doi.org/10.1016/S0920-5861(02)00214-6
[13] K. L. Foon, M. Kashif, U. Hashim, W. W. Liu, Ceramics International, **40**, 753-761, (2014); https://doi.org/10.1016/j.ceramint.2013.06.065
[14] F. Caillaud, A. Smith, J. F. Baumard, J. of the American Ceramic Society, **76**(4), 998-1002, (1993); https://doi.org/10.1111/j.1151-2916.1993.tb05325.x
[15] W. R. Saleh, N. M. Saeed, W. A. Twej, M. Alwan, Advances in Materials Physics and Chemistry, **2**(1), 11-16, (2012); https://www.scirp.org/journal/paperinformation?paperid=17891
[16] B. Gherbi, S. E. Laouini, S. Meneceur, A. Bouafia, H. Hemmami, M. L. Tedjani, G. Thiripuranathar, A. Barhoum, and F. Menaa, Sustainability, **14**(18), (2022), 11300; https://doi.org/10.3390/su141811300
[17] S. Benramache, B. Benhaoua, and F. Chabane, Journal of Semiconductors, **33**(9), (2012). https://iopscience.iop.org/article/10.1088/1674-4926/33/9/093001
[18] A. Beggas, B. Benhaoua, A. Attaf, M. S. Aida, Optik **127**(20), 8423–8430, (2016); https://doi.org/10.1016/j.ijleo.2016.06.030
[19] A. Beggas, Z. Becer, R. Ahmim, M. S. AIDA, Defect and Diffusion Forum, **397**, 125-140 (2019); https://doi.org/10.4028/www.scientific.net/DDF.397.125
[20] R. Wahab, S. G. Ansari, Y. S. Kim, M. Song, H. S. Shin, Applied Surface Science, **255**(9), 4891- 4896 (2009); https://doi.org/10.1016/j.apsusc.2008.12.037
[21] A. Ashok, G. Regmi, A. Romero Nunez, M. Solis Lopez, S. Velumani, H. Castaneda, Journal of Materials Science: Materials in Electronics, **31**, 7499-7518, (2020); https://doi.org/10.1007/s10854-020-03024-3
[22] T. Kamal, F. A. Sohaly, International Journal for Research in Applied Science & Engineering Technology (IJRASET), **6**, 720-725, (2018); https://www.researchgate.net/publication/328902607
[23] H. Onoda, M. Chemel, Cerâmica, **63**, 197-202, (2017); http://dx.doi.org/10.1590/0366-69132017633662149
[24] A. Sakthivelu, S. Valanarasu, and J. J. Prince, Int. J. Chem. Sci, 7(4), 2463-2469, (2009); https://www.tsijournals.com/articles
[25] S. A. Kulkarni, P. S. Sawadh, P. K. Palei, K. K Kokate, Ceram. Int, **40**(1), 1945–1949, (2014) ; http://dx.doi.org/10.1016/j.ceramint.2013.07.103